

University of Groningen

A study on the characteristics of Algerian Hassi-Messaoud asphaltenes

Abbas Abbas, Hadj ; Manasrah, Abdallah ; Carbognani, Lante; Sebakhy, Khaled O.; El Hariri El Nokab, Mustapha; Nassar, Nashaat

Published in:
Petroleum Science and Technology

DOI:
[10.1080/10916466.2021.2017457](https://doi.org/10.1080/10916466.2021.2017457)

IMPORTANT NOTE: You are advised to consult the publisher's version (publisher's PDF) if you wish to cite from it. Please check the document version below.

Document Version
Version created as part of publication process; publisher's layout; not normally made publicly available

Publication date:
2021

[Link to publication in University of Groningen/UMCG research database](#)

Citation for published version (APA):

Abbas Abbas, H., Manasrah, A., Carbognani, L., Sebakhy, K. O., El Hariri El Nokab, M., & Nassar, N. (2021). A study on the characteristics of Algerian Hassi-Messaoud asphaltenes: Algerian Hassi-Messaoud asphaltenes: solubility and precipitation. *Petroleum Science and Technology*, 1-23.
<https://doi.org/10.1080/10916466.2021.2017457>

Copyright

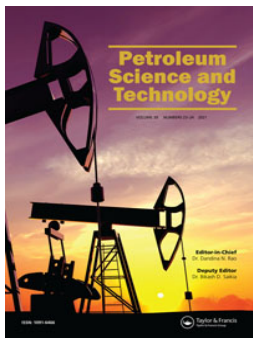
Other than for strictly personal use, it is not permitted to download or to forward/distribute the text or part of it without the consent of the author(s) and/or copyright holder(s), unless the work is under an open content license (like Creative Commons).

The publication may also be distributed here under the terms of Article 25fa of the Dutch Copyright Act, indicated by the "Taverne" license. More information can be found on the University of Groningen website: <https://www.rug.nl/library/open-access/self-archiving-pure/taverne-amendment>.

Take-down policy

If you believe that this document breaches copyright please contact us providing details, and we will remove access to the work immediately and investigate your claim.

Downloaded from the University of Groningen/UMCG research database (Pure): <http://www.rug.nl/research/portal>. For technical reasons the number of authors shown on this cover page is limited to 10 maximum.




A study on the characteristics of Algerian Hassi-Messaoud asphaltenes: solubility and precipitation

Hadj Abbas Abbas, Abdallah D. Manasrah, Lante Carbognani, Khaled O. Sebakhy, Mustapha El Hariri El Nokab, Messaoud Hacini & Nashaat N. Nassar


To cite this article: Hadj Abbas Abbas, Abdallah D. Manasrah, Lante Carbognani, Khaled O. Sebakhy, Mustapha El Hariri El Nokab, Messaoud Hacini & Nashaat N. Nassar (2021): A study on the characteristics of Algerian Hassi-Messaoud asphaltenes: solubility and precipitation, Petroleum Science and Technology, DOI: [10.1080/10916466.2021.2017457](https://doi.org/10.1080/10916466.2021.2017457)



To link to this article: <https://doi.org/10.1080/10916466.2021.2017457>

 View supplementary material 

 Published online: 23 Dec 2021.

 Submit your article to this journal 




 Article views: 43

 View related articles 

 View Crossmark data 



A study on the characteristics of Algerian Hassi-Messaoud asphaltenes: solubility and precipitation

Hadj Abbas Abbas^{a,b}, Abdallah D. Manasrah^{a,c} , Lante Carbognani^a, Khaled O. Sebakhy^d , Mustapha El Hariri El Nokab^e, Messaoud Hacini^b, and Nashaat N. Nassar^a 

^aDepartment of Chemical and Petroleum Engineering, University of Calgary, Calgary, Alberta, Canada; ^bLaboratoire de géologie du Sahara, Université Kasdi Merbah Ouargla, Ouargla, Algérie; ^cCarbon OxyTech Inc., Calgary, Alberta, Canada; ^dDepartment of Chemical Engineering, Engineering and Technology Institute Groningen (ENTEG), University of Groningen, Groningen, The Netherlands; ^eSolid State NMR Spectroscopy Group, Zernike Institute for Advanced Materials (ZIAM), University of Groningen, Groningen, The Netherlands

ABSTRACT





This study focuses on detailed characterizations of asphaltene fractions extracted from the Algerian Hassi-Messaoud oil field. It was found that the extracted asphaltenes are not completely soluble in toluene, instead two fractions of asphaltenes were obtained upon solubilizing the heptane-precipitated neat asphaltenes in toluene. Extensive characterizations of the toluene-soluble and insoluble fractions were carried out using elemental analysis, Fourier transform infrared (FTIR), thermogravimetric analysis (TGA), X-ray diffraction (XRD) and solid-state nuclear magnetic resonance (ssNMR). It was suggested that the high oxygen content and uneven compositional structures are the main contributors to asphaltene instability. The toluene-insoluble fractions were found to have higher polarity and aromaticity as well as more oxygen content than the neat asphaltenes and toluene-soluble fractions.

KEYWORDS

Hassi-Messaoud asphaltenes; instability; ssNMR; toluene-insoluble; toluene-soluble

1. Introduction

Light oil is considered the first source of energy worldwide, and it plays a key role in the economy of many countries (Sagar 2005; Gowdy and Julia 2007; Yoon et al. 2009). Algeria, for instance, has production capacity of crude oil more than 1.4 million barrels per day. As an average producer in OPEC, Algeria ranks 10th in the world; ahead of Qatar and Ecuador (DE and DE Master 2009). Regardless of the high-quality of produced crude oil in Algeria (the Saharan mix), with low density and sulfur content, many

CONTACT Abdallah D. Manasrah  manasrah@carbonoxytech.com  Department of Chemical and Petroleum Engineering, University of Calgary, 2500 University Street NW, Calgary, AB T2N1N4, Canada; Nashaat N. Nassar  nassar@ucalgary.ca  Department of Chemical and Petroleum Engineering, University of Calgary, 2500 University Street NW, Calgary, AB T2N1N4, Canada.

 Supplemental data for this article is available online at <https://doi.org/10.1080/10916466.2021.2017457>.

issues arise during the oil recovery, production and processing due to asphaltene deposition (Boukherissa 2008; DE and DE Master 2009; Larbi et al. 2015; Daaou et al. 2016). Asphaltenes found to be precipitated in different levels; near-wellbore region, wellhead, separators, tubing, and safety valves (Daaou et al. 2016). Although the light oil produced from Hassi-Messaoud Oil Field has low asphaltene content, the asphaltene deposition is significantly recorded and observed during the oil production (Alian et al. 2011; Daaou et al., 2016). In fact, the presence of asphaltenes in the oil matrix is one of the main challenges facing oil production from Hassi-Messaoud Oil Field. The asphaltene deposition contributes to several issues in the utilization and recovery of oil from which led to major complications in the pipelines and wellbores in Algerian petroleum fields, thus many wells have been entirely shutdown (Boukherissa 2008). Such common types of formation damage, precipitation and deposition that are typically caused by asphaltenes in the reservoir and the production system (Leontaritis et al. 1994; Maqbool et al. 2009) are the most difficult to pass. In addition, asphaltene deposition is challenging in many different domains of the oil industry, such as alteration of reservoir rock wettability from water-wet to oil-wet due to its potential to be adsorbed on reservoir rock (Al-Maamari and Buckley 2003; Mohammadi et al. 2017), plugging flow lines because of asphaltene deposit build-up (Creek 2005), and refinery catalyst deactivation because of asphaltene adsorption at active sites (Trimm 1996; Mustafin et al. 2020). Consequently, these asphaltene-related problems cause significant production losses and vastly increase in operational costs. Therefore, a comprehensive study on the characterization of Algerian asphaltenes has to be addressed here to understand its chemical and physical behavior. Despite the importance of Algerian crude oil in the world market, a few studies on the asphaltene characterization were conducted in this manner (Bouhadda et al. 2007; 2010; Daaou et al. 2012; Fergoug and Bouhadda 2014; Larbi et al. 2015). Larbi, et al. (2015), for example, investigated the structural parameters and self-aggregation of two types of Algerian asphaltenes extracted from oil well and storage tank. It was found that the asphaltenes extracted from the storage tank have higher polarity and solubility in aromatics with lower aromaticity compared with the ones extracted from the oil well. Daaou et al. (2016) characterized three types of Algerian asphaltenes collected from different oil sources. The characterization findings indicated that there is a significant difference in the chemical structure of the tested samples especially in the number of aromatic rings, aromaticity factors and heteroatoms. Their study also confirmed that the chemical structure and composition were changed during storage and processing. In another characterization study on the Algerian asphaltenes, it was found that the asphaltene molecules contain seven

condensed rings linked with aliphatic chains of 4–6 carbons (Fergoug and Bouhadda 2014). Bouhadda et al. (2007) described the structural parameters of asphaltenes extracted from the deposit of the Hassi-Messaoud Oil Field in Algeria. Moreover, detailed studies were carried out on the conditions of Algerian asphaltene precipitation in Hassi-Messaoud Oil Field provided by Haskett and Tartera (1965). Their findings demonstrated that the deposition of asphaltenes is more pronounced in the tubing which requires frequent cleaning. Furthermore, several studies have investigated the asphaltenes deposition in Hassi-Messaoud and reported in the literature (Carbognani et al. 2000; Guan et al. 2018).

Nevertheless, the majority of the aforementioned studies did not pay attention to the asphaltene behavior and solubility, and they considered the Algerian asphaltenes following the global definition of asphaltenes, which are completely soluble in aromatics. However, this is not the case in our present study, where the Algerian asphaltenes were found to be partially insoluble in aromatics like toluene. Asphaltenes are solubility class materials and globally defined as the heaviest, most aromatic and surface-active fraction of the crude oil, being insoluble in light paraffin like n-pentane (n-C₅), n-hexane (n-C₆) and n-heptane (n-C₇), but soluble in light aromatics like benzene, toluene or pyridine (Mullins 2011; Mullins et al. 2012; Adams 2014). The “solubility class” definition of asphaltenes generates a broad distribution of molecular structures that can vary greatly from one crude oil to another. Generally, asphaltenes have a polyaromatic structure that includes a few alkyl groups per aromatic ring and polarheteroatom-containing functional groups, such as nitrogen, sulfur, oxygen, and several metallic heteroatom, such as V, Fe, and Ni (Groenzin and Mullins 2000; Schuler et al. 2015). Therefore, the presence of functional groups such as carboxyl, ketones, aldehydes, benzothiophenes, dibenzothiophenes, naftenobenzothiophenes, alkyl sulfides, aryl alkyl sulfides, and aryl sulfides are likely to occur in asphaltene structure (Groenzin and Mullins 1999; Mullins 2011; Schuler et al. 2017a). Although the structure of asphaltenes is complex, several hypotheses on asphaltene chemical structures are proposed in the literature; including island, archipelago, continental, or rosary-type (Acevedo et al. 2007; Durand et al. 2010; Mullins et al. 2012; Schuler et al., 2017b). The island architecture is composed of seven fused rings and one polyaromatic hydrocarbon (PAH’s); while the archipelago architecture is composed of more than one PAH per asphaltene molecule connected by alkyl chains (Murgich 2003; Mullins et al. 2012). The continental architecture is composed also by one or two PAH’s but with a larger number of fused rings than seven (Murgich 2003; Durand et al. 2010). The rosary-type asphaltenes are very flexible and are composed of two or more PAH’s joined by flexible aliphatic chains

Table 1. Elemental analysis of Algerian Hassi-Messaoud neat asphaltenes and toluene-insoluble and soluble fractions after dissolving 1 g of neat asphaltenes sample in 400 mL toluene.

Content	Types of asphaltenes					
	(AS) _{OR}		(AS) _{NS}		(AS) _S	
	(wt.%)	Mass, mg	(wt.%)	Mass, mg	(wt.%)	Mass, mg
C	88.68	886.8	86.15	387.67	89.2	490.6
H	5.89	58.9	5.42	24.39	6.88	37.84
N	1.36	13.6	1.02	04.59	0.46	2.53
S	1.80	18.00	1.29	5.81	1.15	6.33
O	2.27	22.7	6.12	27.54	2.31	12.70
Total (mg)		1000		450		550
Total heteroatoms (wt.%) [*]		5.43		8.43		3.92
H/C atomic		0.79		0.75		0.92
Metals (ppm)						
Ni		99.5		99.32		99.35
V		82.8		83.02		83.07
Fe		91.15		90.89		90.21

^{*}Total heteroatoms = O + S + N.

(Schuler et al. 2020). However, owing to its complex chemical structure, asphaltene architectures get updated with time.

Herein, our study presents a first attempt to characterize the toluene soluble and insoluble fractions of Algerian Hassi-Messaoud asphaltenes and investigate the role of heteroatoms especially the oxygen content in the asphaltenes structure which we believe is playing a major role in asphaltene precipitation. Thus, it was noticed that the extracted Algerian Hassi-Messaoud asphaltenes are partially insoluble in toluene, which may seem contradictory to the global definition of asphaltenes. Therefore, we carried out detailed characterizations for the neat asphaltenes (AS)_{OR}, soluble fraction in toluene (AS)_S and insoluble fraction (AS)_{NS} using FTIR, TGA, XRD, ssNMR, and elemental analysis.

2. Experimental work

2.1. Materials

An oil sample was obtained from the Hassi-Messaoud Oil Field, located in the southeastern Algeria, and was used in this study as the source of Algerian asphaltenes. The crude oil for this field has 45° API (specific gravity of 0.802), viscosity of 2.51 mPa.s at 20 °C and 0.6 (w%/w%) of asphaltenes content (Daaou et al. 2016). Table S1 in the Supplementary Materials provides a full saturates, aromatics, resins, and asphaltenes (SARA) analysis of the oil (Abbas et al. 2021). n-heptane (99%) was used as a solvent for neat asphaltenes extraction from Algerian light oil and toluene HPLC grade was used as a solvent to solubilize the neat asphaltenes sample. Both solvents were obtained from Sigma-Aldrich, Ontario, Canada and used as received.

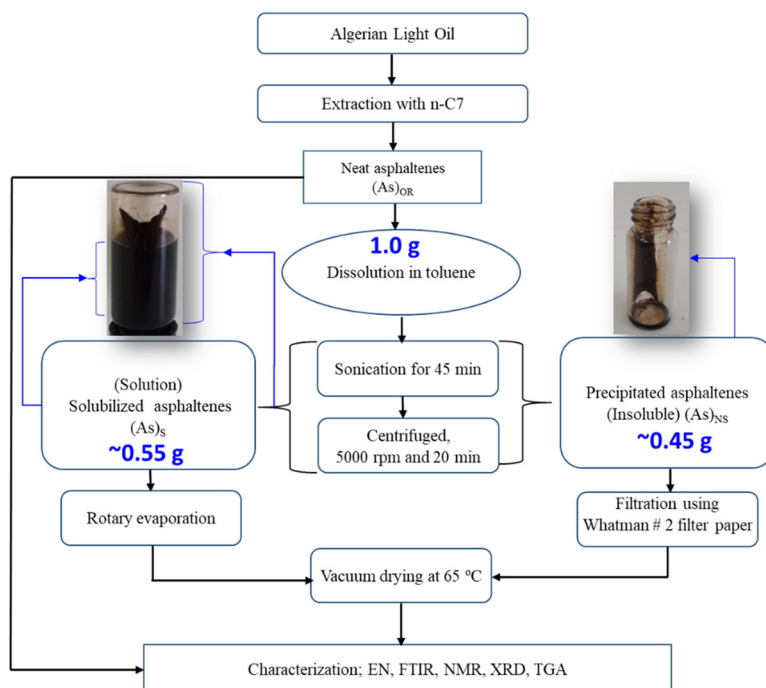


Figure 1. Schematic representation of toluene-soluble and insoluble asphaltene extraction. The upside-down vial on the left represents the neat asphaltene in toluene (500 ppm) and the vial on the right shows the insoluble asphaltenes after decanting the supernatant.

2.2. Extraction protocol of neat asphaltenes

Asphaltenes were extracted from the Hassi-Messaoud Oil Field sample based on the ASTM D2892 and ASTM D5236 procedure (D5236-13, A 2013; D2892-16, A 2016). The extraction experiments were performed by adding n-heptane to the oil with a 1:40 (g/mL) oil/solvent ratio (O/S). Then, the mixture was heated to 100 °C in a round-bottom flask. After that, the mixture was settled for 45 min at room temperature for precipitation. The solution was filtered using Whatman No. 2 filter paper. The precipitated asphaltenes were washed with n-heptane at a 1:5 (O/S) ratio until the solvent became colorless. This washing step helped to remove all the precipitates from the flask wall and ensured that the solids were well deposited on the filter paper. Then, the filtered asphaltenes (neat one) were dried under vacuum in an oven at 65 °C for 30 min.

2.3. Isolation of toluene-soluble and insoluble asphaltenes

The toluene-soluble fraction of asphaltenes (AS)_S and toluene-insoluble fraction (AS)_{NS} were obtained by exposing 1.0 g of neat asphaltenes to 400 mL toluene. Figure 1 shows a schematic representation of the isolation steps of (AS)_S and (AS)_{NS} from the neat asphaltenes (AS)_{OR}. After adding

the neat asphaltenes into toluene, the solution was ultrasonicated for 60 min and then allowed to stand at room temperature for 5 h (as shown in the upside-down vial on the left of Figure 1). The solution was then centrifuged (Eppendorf centrifuge 5804) at 5000 rpm for 20 min to separate the insoluble fraction of asphaltenes, which was collected using Whatman filter paper and dried at 25 °C (the right vial in Figure 1). The supernatant which contains the soluble fraction was then evaporated using a rotary evaporator to recover the soluble fraction of asphaltenes in toluene. It is worth mentioning that different concentrations of neat asphaltenes were prepared to confirm the solubility of asphaltenes in the toluene and to make sure that the precipitated asphaltenes (insoluble one) are obtained before the precipitation onset. Even at low concentration (<10 mg/L) the precipitation of asphaltenes was noticed.

2.4. Characterization of different fractions of asphaltenes

2.4.1. Elemental analysis

The elemental analyses (carbon, hydrogen, nitrogen, oxygen and sulfur) for the different fractions of toluene-soluble and insoluble asphaltenes, as well as the neat sample, were identified. Around 1.5 mg of each sample were used. All the measurements were performed in triplicate with $\pm 0.02\%$ relative standard deviation.

2.4.2. Infrared spectroscopy

The chemical functionalities of the isolated solid samples were characterized by a Shimadzu IR Affinity-1S FTIR (Mandel, USA). The FTIR is provided with a smart diffuse reflectance attachment to carry out diffuse reflectance infrared Fourier transform spectroscopy (DRIFTS) analysis. The background was first performed using 500 mg powder of pure potassium bromide (KBr), then approximately 500 mg of KBr were mixed with 5 mg of asphaltenes. The resulting mixture was grinded using an agate mortar and pestle for homogenizing the sample. The IR spectra were obtained in the wavenumber ranging from 400 to 4000 cm^{-1} . All the spectra were acquired as averages of 50 scans with a resolution of 4 cm^{-1} .

2.4.3. Thermogravimetric analysis

The thermo-oxidative decomposition of the different asphaltene fractions was investigated using a thermogravimetric TGA/DSC analyzer (SDT Q600, TA Instruments, Inc., New Castle, DE). ~ 5 mg of each fraction was heated from 25 to 800 °C with a heating rate of 10 °C/min under the air flow of 100 cm^3/min .

2.4.4. X-Ray diffraction

The X-ray analysis was performed using a Rigaku Ultima III Multi-Purpose Diffraction System X-ray diffractometer (Rigaku Corp., The Woodlands, TX) with Cu K α radiation as the X-ray source. The scan ranged from 3 to 90° 2 θ degrees using a 0.02° step and a counting time of 0.2 step/s. The analysis was operated at 40 kV and 44 mA to obtain the full diffractogram for each analyzed material.

2.4.5. Solid-state nuclear magnetic resonance

The NMR experiments were carried out on a Bruker Avance Neo FT-NMR spectrometer equipped with a narrow-bore 14.1 T magnet and a 4 mm broadband magic angle spinning (MAS) probe. The corresponding Larmor frequency was 600.130 and 150.903 MHz for ^1H and ^{13}C , respectively. All experiments were conducted in 4 mm zirconia rotors at spinning rate of 10 kHz and 293 K (setpoint temperature). Spectra were referenced to the ^{13}C chemical shifts of adamantane and processed by MestReNova 12.0.0-20080. The ^1H single pulse experiments were done with a 4 μsec 90° pulse length, nutation frequency 42.5 kHz, 4 s repetition delay, and 64 scans. The ^{13}C single pulse experiments were done with a 5 μs pulse length, nutation frequency 50 kHz, 45 s repetition delay, 2048 scans and a proton TPPM decoupling pulse with frequency of 50 kHz.

3. Results and discussion

3.1. Elemental analysis of neat and toluene-insoluble and soluble asphaltenes

The H/C ratio, one of the key parameters that identify the degree of aromaticity of the Algerian asphaltenes and its fractions, was evaluated for the three samples of asphaltenes. Theoretically, the value of H/C ranges from ~ 2 for long alkyl chains to around unity for species like benzene and to less than unity, such as the condensed aromatic rings. To investigate this parameter, Table 1 shows the quantification of hydrocarbon (C and H), heteroatoms (N, S, and O) and metals along with H/C ratios for the three asphaltene fractions. As shown, the higher value of H/C ratio was recorded in (AS)_S sample (0.92), suggesting a lower contribution of aromaticity compounds compared with the (AS)_{OR} and (AS)_{NS} (Calemma et al. 1995; Midttum, 1999). The lower value of H/C ratio was recorded in the toluene insoluble fraction (AS)_{NS} (0.75), featuring higher aromaticity involving a bigger number of substituted aromatic structures. These features have been taken into account in the determination of solubility. Acevedo et al (2004) reported that the aromaticity plays a significant role in solubility and their results suggested that the fractions that have more aromaticity have a complex structure and low solubility.

Table 2. The corresponding aromatic (A_3/A_1) and carbonyl (A_2/A_1) indexes for the Algerian Hassi-Messaoud neat asphaltenes and toluene-insoluble and soluble fractions.

Sample	A_3/A_1	A_2/A_3
(AS) _{OR}	0.51	1.25
(AS) _{NS}	0.71	1.15
(AS) _S	0.45	1.40

However, the fractions with low aromaticity have a high solubility because of more flexible structures in presence of several aliphatic chains (Acevedo et al. 2004). As reported, the higher the value of H/C ratio the longer aliphatic chains in the asphaltene (Leyva et al. 2013). The obtained values of H/C for all tested asphaltene fractions are lower than the reported value for the Algerian asphaltenes in different studies, indicating that our extracted asphaltene fraction at that location is more aromatic (Bouhadda et al. 2000). The table also shows a slight difference in C and H content was found in the three samples, while the (AS)_{NS} has a slight lower amount of carbon. The oxygen content is significantly larger than the content of the other heteroatoms in all samples. Importantly, the (AS)_{NS} has the highest polarity among all samples, which could be attributed to its high oxygen content (6.12 wt%), while the other two samples showed lower amount of oxygen \sim 2.27 and 2.31 wt% for the (AS)_{OR} and (AS)_S, respectively. The nitrogen and sulfur contents correspond to usually observed values in the Algerian crude oils (Daaou et al., 2008; Bouhadda et al. 2010). The (AS)_{OR} sample has the highest sulfur content while no difference in sulfur content could be observed in (AS)_S and (AS)_{NS} samples. In comparison, the elemental composition of Algerian Hassi-Messaoud asphaltenes is remarkably similar to world extracted asphaltenes with lower sulfur content and much lower H/C ratio. The elemental compositions of various asphaltenes from Canada, Iran, Iraq, and Kuwait are compared in Table S2 in the Supplementary Materials. Based on the elemental analysis, it can be determined that the Algerian Hassi-Messaoud asphaltenes has H/C atomic ratio between 0.75 and 0.92 with considerable content of heteroatoms, more oxygen in the (AS)_{NS}. Considering the average molecular weight of asphaltenes ranges from 500 to 1000 Da (Acevedo et al. 2007), it can be concluded that the asphaltenes backbone consists of fused aromatic carbons interspersed with polar functional groups containing a few heteroatoms per molecule. This finding was also supported by Spiecker et al. (2003) who found that the asphaltenes structure contains five to seven heteroatoms per molecule for the atomic H/C ratio ranges between 1.0 and 1.2, and with a few weight percent of heteroatoms (Spiecker et al. 2003). Such findings have been also reported by Medina et al. (2020) as the asphaltenes with a lower polarity contain higher H/C ratio with higher aliphatic groups (Medina et al. 2020). Worth mentioning here that the content of heteroatoms (N + S + O) is another factor that increases the polarity of asphaltenes (Yao et al. 2020).

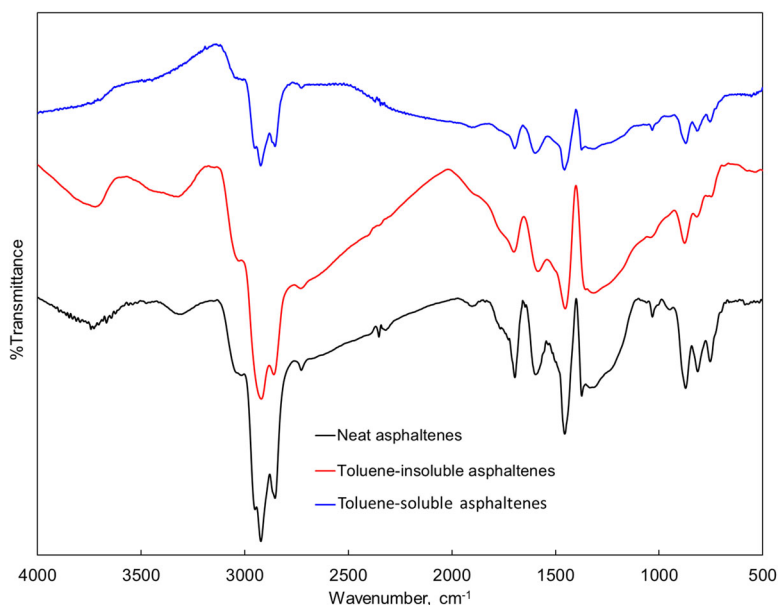


Figure 2. FTIR spectra for the neat, toluene-soluble, and toluene-insoluble asphaltenes.

As shown in the [Table 1](#), more content of heteroatoms can be observed in (AS)_{NS} sample. Nevertheless, the metal analysis of the three samples showed that both nickel and vanadium form complexes of the porphyrin type with the pyroles (Strausz et al. 1992; Freeman et al. 1993).

3.2. FTIR analysis

FTIR analysis was carried out for the neat asphaltenes, toluene-insoluble and toluene-soluble asphaltenes to investigate their chemical structure and functionalities. [Figure 2](#) shows the IR-spectra of the three samples. As seen, the presence of hydrocarbon functions, that is, alkyls ($3000\text{--}2800\text{ cm}^{-1}$) and aromatics (3050 and $950\text{--}750\text{ cm}^{-1}$) are observed in all samples. However, a significant difference in the intensity could be observed. For the neat asphaltenes, in the aliphatic region, the presence of --C--H asymmetric and symmetric stretching (--CH_3 , =CH_2 and $\text{--CH}_2\text{CH}_3$) can be assigned in the region of $2852\text{--}2935\text{ cm}^{-1}$. The bending vibrations of --C--H were identified at $1375\text{--}1377\text{ cm}^{-1}$ (Manasrah et al. 2019b). In the aromatic region, the presence of C–H bonds vibration out-of-plane in aromatics was assigned between 717 and 873 cm^{-1} bands. The corresponding C=C aromatic stretching vibration appears near 1614 cm^{-1} while the aromatic C–H stretching presented in the weak band at 3040 cm^{-1} . Worth noting that the presence of N–H and --OH functionalities were observed in the spanning broad bands from 3320 cm^{-1} and its corresponding bond signals at ($2800\text{--}2000\text{ cm}^{-1}$). The presence of C=O carbonyl stretching is possible here which is assigned at

Table 3. The crystalline parameters for neat, toluene-soluble, and toluene-insoluble asphaltenes obtained from XRD diffractograms.

Crystalline parameter	Neat Asphaltenes	Toluene-soluble asphaltenes	Toluene-insoluble asphaltenes	Equations	References for the considered equation
f_a	0.42	0.44	0.46	$f_a = \frac{A_{002}}{A_{002}+A_\gamma}$	(Hung et al. 2017)
d_m , Å	3.52	3.49	3.52	$d_m = \frac{\lambda}{2 \sin \theta_{002}}$	(Lei et al. 2018)
d_γ , Å	6.11	5.96	5.69	$d_\gamma = \frac{5\lambda}{8 \sin \theta_\gamma}$	(Lei et al. 2018)
L_a , Å	29.93	15.97	17.07	$L_a = \frac{1.84 \lambda}{\omega \cos \theta_{10}}$	(Fini et al. 2017)
L_c , Å	13.99	13.83	13.04	$L_c = \frac{0.9\lambda}{\omega \cos \theta_{002}}$	(Lei et al. 2018)
M	4.97	4.96	4.70	$M = \frac{L_c}{d_m} + 1$	(Fini et al. 2017)
R_a	13	7	7	$R_a = \frac{L_a}{2.667}$	(Fini et al. 2017)
C_{AU}	32	17	18	$C_{AU} = \frac{L_a+1.23}{0.65}$	(Hung et al. 2017)

1683 cm^{-1} . Moreover, the presence of sulfoxide species is assigned at 1030 cm^{-1} with high intensity indicating a higher contribution of sulfur in the neat sample in comparison with the other fractions which also confirmed by the elemental analysis. These findings led us to conclude that the structure of the neat asphaltenes is similar to those Algerian asphaltenes reported in the literature (Daaou et al. 2009; Larbi et al. 2015).

Similarly, the spectra of toluene-soluble and insoluble asphaltenes fractions were found to coincide with the neat asphaltenes with some changes in the features and intensity. As shown, the broad bands at 3320 and 3600 cm^{-1} are hardly visible in the toluene-soluble asphaltenes compared with the neat and toluene-insoluble samples. Another important feature in the toluene-soluble asphaltenes is the lower intensity of sulfoxide band at 1030 cm^{-1} . These findings also supported by the elemental analysis results where the toluene-soluble asphaltenes have the lowest sulfur content compared with the toluene-insoluble and neat sample. Another difference is the presence of C–H deformation bond at 1373 cm^{-1} in both neat and toluene-soluble samples which is absent in the insoluble one. Importantly, the presence of carbonyl group (C=O) in the toluene-insoluble sample is confirmed by the well-defined peak around 1700 cm^{-1} suggesting the presence of ketone or aldehyde functionality (Manasrah and Nassar 2020). These findings confirm the presence of high content of oxygen in this sample. Table S3, in the Supplementary Materials, summarizes the FTIR bands with their assigned frequencies and intensity for the three samples. The IR results reveal that there are many groups capable of forming oxygen bonds, especially in the toluene-insoluble sample, including carboxylic acids, carbonyls, phenols, and sulfoxide in addition to the nitrogen groups such as pyrrolic and pyridine. These hydroxyl groups would exist almost entirely as intramolecular hydrogen-bonded complexes where the later bonds are capable of donating or accepting protons inter- and intramolecularly. Thus, the presence of these oxygen and nitrogen functionalities in asphaltene structures may reduce their solubility in toluene by increasing their polarity. It is worth mentioning here

that the water alternating gas (WAG) process is used nowadays for enhanced oil recovery in the Algerian oil field instead of natural gas flooding. The latter technique is no longer used due to commercial considerations, as Algeria exports gas to southern European countries. Water flooding is also used as a solution to the problems of salt deposition. Therefore, water is likely to be the primary source of oxygen content in asphaltenes. Additional sources for oxygen could be related to the reformat, a petroleum distillate produced locally in Algeria. The reformat obtained by this method is essentially constituted by paraffins, naphthenes, and aromatics (PNA) with composition of 42, 5, and 53 wt.%, respectively. Moreover, the presence of CO₂ due to the gas injection into the reservoir could be another source of oxygen in asphaltenes, for the case of gas flooding.

To better understand the characteristic feature of these fractions, the degree of aromaticity and carbonyl concentration were also considered here by integration of the areas under the aliphatic stretching absorption in the range 3100–2770 cm⁻¹ (A₁), the carbonyl stretching absorption in the range 1800–1630 cm⁻¹ (A₂), and the aromatic C=C stretching vibrations in the range 1650–1520 cm⁻¹ (A₃). Consequently, the ratios A₃/A₁ and A₂/A₃ are evaluated and presented in Table 2. Worth noting that the A₃/A₁ ratio indicates the degree of aromaticity while A₂/A₃ ratio implies the carbonyl concentration per unit of aromatic structure. As shown in the table, the (AS)_{NS} sample has higher aromaticity and lower carbonyl concentration in comparison with (AS)_{OR} and (AS)_S. The toluene-soluble fraction has lower aromaticity and higher carbonyl concentration compare with the neat asphaltenes. The values of these ratios in the neat asphaltenes are within the same range as reported for the Algerian asphaltenes indicating the high aromaticity and polarity (Larbi et al. 2015). These results led us to conclude that the structure of toluene-insoluble and soluble asphaltenes were found to be similar to the original asphaltenes with some features changed due to the contribution of aromatic degree and the intensity of heteroatoms, especially the oxygen content which might affect the polarity of toluene-insoluble asphaltenes. It was reported that high contribution of oxygen functionalities in asphaltenes structure, such as COO groups, have a significant effect on increasing the oxygen content through chemisorption (Medina et al. 2020). These findings are also confirmed by increasing the degree of aromatization which associated with the decreasing of alkylation degree, thus increases the amount of oxygen as reported by Medina et al. (2020).

3.3. TGA/DSC analysis

To gain insights into the differences of the considered asphaltene fractions, thermal analysis of asphaltene fractions was performed.

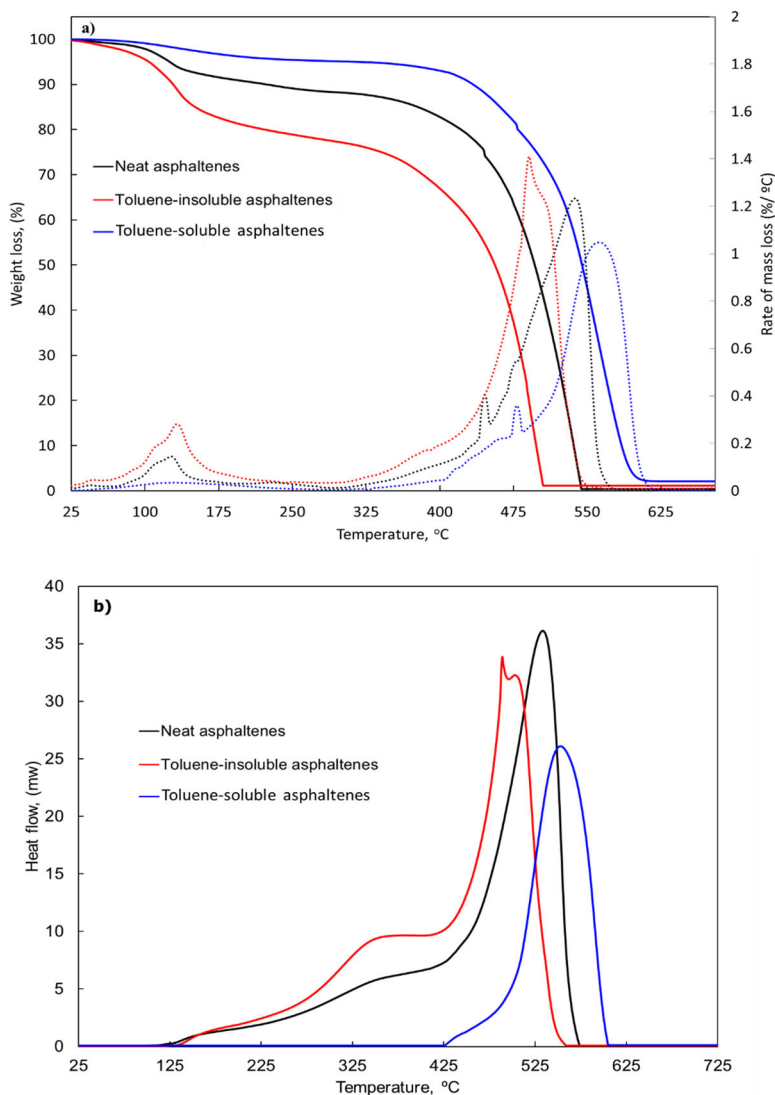


Figure 3. TGA-DSC plots of neat, toluene-soluble and toluene-insoluble asphaltenes, (a) weight loss and rate of weight loss as a function of temperature, (b) heat flow change with temperature at a heating rate of 10 °C/min and air flowrate of 100 cm³/min.

Figure 3a,b shows the profiles for the mass loss along with its derivatives and heat changes, respectively, for neat, toluene-soluble, and insoluble asphaltenes under air atmosphere with a heating rate of 10 °C/min. As seen, the three samples were completely burned off at different oxidation temperatures having a maximum weight loss at 506, 550, and 609 °C for (AS)_{NS}, (AS)_{OR}, and (AS)_S, respectively. As shown in the mass loss for neat asphaltene sample, a smooth %weight decrease is observed from 230 to 390 °C followed by a fast reduction of %weight in a relatively narrow range (390–470 °C). The total volatilization of

asphaltenes was achieved at 535 °C, thus asphaltenes at this temperature were fully burned off in the presence of air.

The rate of mass loss profile indicates that the oxidation of original asphaltene occurs in three regions. Regardless of the small peak from 70 to 150 °C which refers to moisture and residual solvent used in the extraction (Trejo et al. 2010), the first oxidation peak starts from 300 to 400 °C which attributed to the oxidation of the paraffinic chains. At this peak, no significant mass change was observed because of the heavy structure of asphaltenes. Another important peak was recorded at 445 °C which could be attributed to dissociation of weaker chemical bonds such as sulfur bridges S–C and N–C (Boukherissa 2008; Trejo et al. 2010). A similar oxidation peak can be observed in toluene-soluble fraction at 480 °C, however, not observed in the toluene-insoluble fraction. The significant mass loss can be observed at around 538 °C due to the complete oxidation of the asphaltenes, and thus transformed to CO₂ and other gases (Nassar et al. 2011). The profiles of heat flow shown in Figure 3b are comparable reflecting similar effects. The presence of exotherm peaks in Figure 3b confirmed the oxidation of asphaltenes. Similar oxidation steps can be observed for the soluble sample with a clear shift to the right, that is, higher oxidation temperature.

The dissociation of chemical bonds such as sulfur bridge S–C and N–C was recorded at 480 °C with insignificant mass loss peak. The intensity of peak corresponding to the maximum rate of mass loss was recorded for toluene-soluble at 570 °C, which means that the oxidation occurred at a higher temperature in comparison with the neat and toluene-insoluble fraction. Worth noting here that no water and residual solvent can be observed in the soluble asphaltenes as indicated in the original and insoluble asphaltenes between 30 and 150 °C. This observation is expected as the extraction method for obtaining the soluble asphaltenes, as represented in Figure 1, would evaporate the water and residual solvent. The presence of an exotherm (Figure 3b) confirmed that the oxidation of the three fractions occurred. On the other hand, the oxidation of the toluene-insoluble fraction occurred at much lower temperatures and took its place in two major steps only. The lower oxidation at 355 °C and higher oxidation at 492 °C, where the latter one corresponds to the maximum rate of mass loss. Importantly, the oxidation temperature of the toluene-insoluble asphaltenes was shifted to a lower temperature in comparison with the neat and toluene-soluble fraction, which can be attributed to the presence of more oxygenated compounds in that fraction. It was reported in our previous study that the oxidation temperature of the hydrocarbons saturated with oxygen like oxy-cracked petroleum coke is much lower than the one with less oxygen content (Manasrah et al. 2018; Manasrah et al. 2019a). These findings agree well with the elemental analysis where the

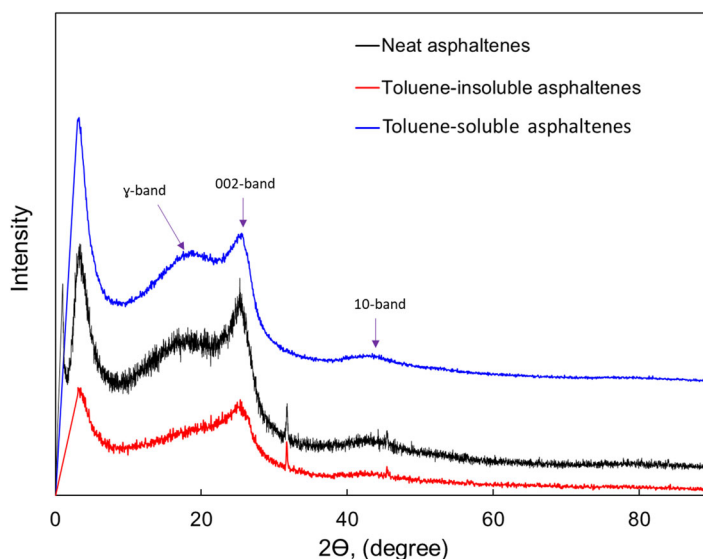


Figure 4. X-ray diffraction patterns for neat, toluene-soluble, and insoluble asphaltenes.

toluene-insoluble fraction has more oxygen content than the neat and toluene-soluble fraction.

3.4. X-Ray diffraction

The X-ray diffraction patterns of neat, toluene-soluble, and insoluble fractions are shown in Figure 4. As seen, the spectrum of neat asphaltenes reflects in five well-defined bands. A strong and sharp band (at $2\theta = 3.42^\circ$) which corresponds to the aliphatic chains or paraffin, γ -band at $2\theta = 17^\circ$ and (002) band at $2\theta = 25^\circ$, the last two bands indicate the saturated and aromatic structures, respectively (Yen et al. 1961). Another sharp band at $2\theta = 32^\circ$ which indicates the presence of silicon oxide SiO_2 . The final band is (10) at $2\theta = 43^\circ$ arises from the reflection in the X-ray pattern by in-plane of the aromatic structure (Siddiqui et al. 2002). Similar peaks were reported for the Algerian Hassi-Messaoud asphaltenes by Daaou et al. (2009), however, no bands were observed at $2\theta = 32^\circ$. On the other hand, similar bands can be observed in the toluene-soluble and insoluble fractions, however, the band at $2\theta = 17^\circ$ is barely visible in the toluene-insoluble fraction and the band at 32° is no longer exist in the toluene-soluble fraction. Worth noting that the observed peaks in the X-ray diffraction spectrum are attributed to the presence of crystalline part in the asphaltene structure such as the long-chain n-paraffins which coprecipitated with asphaltene.

Furthermore, comparing the structural parameters of the three asphaltene fractions, several crystallite parameters were obtained from the XRD

patterns. The aromaticity (f_a), the spacing of the layer between aromatic sheets (d_m), the distance between two saturated chains ($d\gamma$), the diameter of the aromatic planar sheet (L_a), the average height of the crystallite (L_c), the average number of the aromatic sheets (M) per one cluster, the average numbers of aromatic rings in one aromatic sheet (R_a), and the number of carbons per aromatic structural (C_{AU}) have been estimated following the equations detailed in Table 3. The layer spacing between two aromatic sheets (d_m) was calculated using Bragg's equation from the maximum of the graphene (002) band while the distance between two aliphatic chains ($d\gamma$) was estimated using the same equation at θ_γ by considering the wavelength (λ) of Cu K- α radiation equals to 1.54059 Å.

It was previously reported that the asphaltene structure is consisting of repeating units of stacked condensed aromatic sheets controlled by the π - π stacking interactions. According to XRD analysis, the three fractions of asphaltene displayed an average interlayer distance, d_m , in the same range of 3.5 Å. Similarly, the distance between two saturated chains ($d\gamma$) of the asphaltene fractions are not significantly changed and estimated in the same order of 6.00 Å, however, slightly lower for the insoluble sample (3.53 Å) compare with the other samples. These estimated values of both parameters (d_m and $d\gamma$) for our asphaltenes fractions have values within the typical range of the solid petroleum asphaltenes like Saudi crude asphaltenes (Shirokoff et al. 1997) and are slightly smaller than the parameter reported in the resinous-asphaltene components (Kam'yanov, et al. 1989). On the other hand, the average layer diameter of the planar sheets (L_a) was 29.93, 15.97, and 17.07 Å for neat, toluene-soluble, and toluene-insoluble asphaltenes, respectively. This parameter has critical feature in estimating the average number of aromatic rings per sheet in the asphaltene molecule. Thus, the estimated R_a numbers following the same trend, more aromatic per sheet can be found in the neat sample (13) and an identical number of rings (7) were estimated for both toluene-soluble and toluene-insoluble asphaltenes. Furthermore, the average height of the crystallite (L_c) values for all the sample were almost identical in the three fractions of asphaltenes, range from 13 to 14 Å, and insignificant change in the average number of the aromatic sheets (M) was recorded, which are 4.97, 4.96, and 4.70 for neat asphaltenes, toluene-soluble asphaltenes and toluene-insoluble asphaltenes, respectively. However, high number of carbons per aromatic structural, C_{AU} , was obtained for the neat sample (32 atoms) while almost half of this value was obtained for the soluble and insoluble samples. These findings are in good agreement with those reported in the literature (Andersen et al. 2005; Bava et al. 2019). Moreover, the aromaticity (f_a) was obtained by the ratio of the areas of (002) and the sum of (002) and γ bands and fitted using Gaussian approach. The results exhibit that the

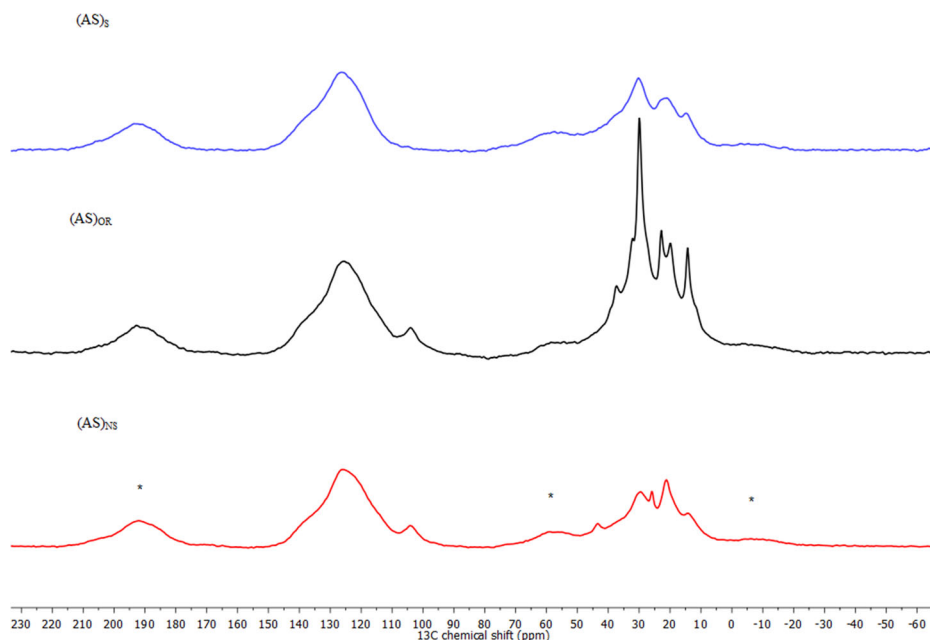


Figure 5. Comparison of ^{13}C 1D spectra for $(\text{AS})_{\text{NS}}$, $(\text{AS})_{\text{OR}}$ and $(\text{AS})_{\text{S}}$ asphaltene samples using ^{13}C single pulse experiment with proton decoupling: Intensity normalized to aromatic signal. *Spinning sidebands for the aromatic region.

aromaticity (f_a) for the three samples are in the same range, however, slightly high for the toluene-insoluble asphaltenes (0.46) compare with the toluene-soluble and neat asphaltenes. Yen et al. (1961) reported that the lower value of (f_a), the lower the aromaticity value. Thus, this might explain that the crystalline part of insoluble asphaltenes has long-term of aromatic rings. Although the X-ray analysis is only referred to the crystalline section of the whole asphaltenes structure, the aromaticity values coincide with the aromaticity results obtained from the elemental analysis and FTIR. Generally, the total aromaticity of asphaltenes has been reported in the range between 0.4 and 0.6 (Andersen et al. 2005). This leads us to conclude that the aromatic rings in the insoluble sample are more compact and condense compared with other tested samples of asphaltenes.

3.5. Solid state NMR analysis

Figure 5 shows the ssNMR spectra for the three samples of asphaltenes. It should be noted that the NMR spectra of the samples were normalized in order to have the same intensity of the aromatic peak, thus the comparison of the aliphatic peaks becomes easier. The NMR spectrum of neat asphaltenes shows multiple signals characteristics of the main aliphatic chains bonded with methyl and methylene groups at chemical shifts of 29.6, 21.1, and 14.4 ppm, and similar peak shapes presented for the $(\text{AS})_{\text{S}}$ and $(\text{AS})_{\text{NS}}$

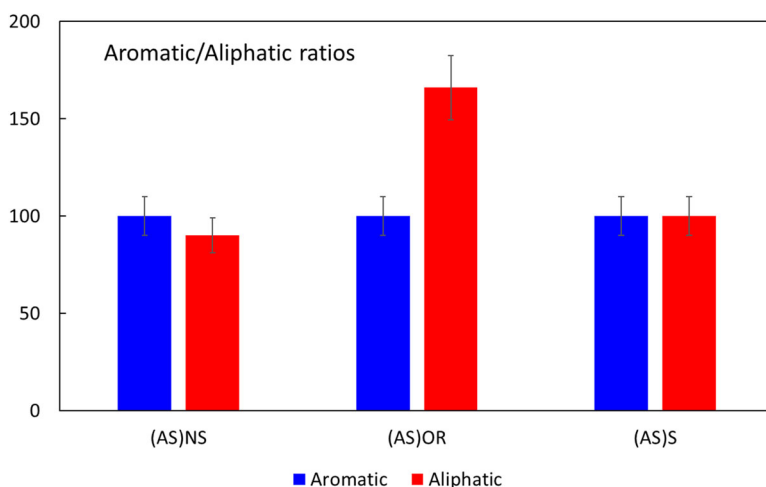


Figure 6. Comparison of aromatic and aliphatic integrated signals for (AS)_{NS}, (AS)_{OR}, and (AS)_S asphaltene samples using ^{13}C single pulse experiment with proton decoupling; Intensity normalized to aromatic signal.

with less intensity. However, in the (AS)_{OR} sample many more peak components were present such as at 19.8, 22.8, 32.2, and 37.5 ppm where the last two peaks represented the methylene groups bonded to the aromatic molecules which are more dominant with shape compared to the aforementioned samples (AS)_S and (AS)_{NS}. In the (AS)_{OR} sample, the methyl groups are more flexible. On the other hand, aromatic peak components such as alkyl-substituted aromatic carbons/internal carbons of condensed aromatic compounds appeared at chemical shifts of 138, 126 ppm. Similar peak shapes were observed for all three samples except for a peak at 104 ppm assigned for anomeric carbon atoms that appear only in the (AS)_{OR} and (AS)_{NS} and having higher intensity in the latter sample. This peak at 104 ppm is corroborated to the di-oxygen substituted aliphatic carbon and anomeric carbon (Lindon et al.2016). Additionally, the presence of oxygenated groups is also presented in all samples. The peak at 45 ppm which is assigned for the methyl ester is only appeared in the (AS)_{NS}. Additionally, sharp peaks present in (AS)_{OR} sample and not present in the other two samples (AS)_{NS} and (AS)_S indicate very different structures/dynamics within the sample in the aliphatic domains. Figure 6 also shows an interesting finding that (AS)_{NS} asphaltene fractions were found to be enriched in aromatics. These findings agree with A_3/A_1 ratio determined via IR spectroscopy and the elemental analysis where the toluene-insoluble asphaltenes fraction contains more oxygen than the other two samples.

The (AS)_{OR} sample seems to have quite different conductance and seems to have a different chemical composition in the aliphatic parts of the sample. At first glance, there is not a huge difference in the aromatic/aliphatic

ratio between these samples. Purely for the aromatic/aliphatic analysis, [Figure 5](#) may be referred to, which employs an analogous approach to the work conducted by Bouhadda et al. (2007). [Figure 6](#) shows a comparison of the aromatic and aliphatic signals for the (AS)_{OR}, (AS)_S, and (AS)_{NS} asphaltene fractions using ¹³C single pulse experiment with proton decoupling. Error bars represent the noise calculated from signal to noise ratio over the entire spectrum. As shown, the aromatic to aliphatic ratio is the highest in the (AS)_{NS} sample. However, the aromatic/aliphatic ratio is significantly lower in the (AS)_{OR} sample compared to the (AS)_S and (AS)_{NS} samples, as depicted in [Figures 5](#) and [6](#). As reported, the high value of aromatic to aliphatic ratio shows extensive substitution of peripheral aromatic carbons which suggest strongly rigid and flat core formed by fusion of polycyclic aromatic and naphthenic units (PANU) as in (AS)_{NS} sample (Gutiérrez et al. 2001; Acevedo et al. 2004). In contrary, the (AS)_S shows lower value of aromatic to aliphatic ratio suggesting more flexible structure of smaller PANU joined the aliphatic chains.

Based on that, we believe that the solubility of asphaltenes in toluene is mainly affected by several structural characteristics, such as polarity, oxygen and heteroatoms content. However, the way the PANU are assembled could be the most dominant factors in changing the solubility of asphaltenes in toluene (Acevedo et al. 2004).

4. Conclusion

The extracted Algerian asphaltenes from Hassi Messaoud Oil Field following the ASTM method was fully investigated in this study after being partially solubilized in toluene. Three samples of asphaltenes, neat asphaltenes that extracted from the oil sample, the toluene-soluble and toluene-insoluble asphaltenes were characterized using elemental analysis, FTIR, TGA, XRD, and ssNMR. The H/C ratio showed that the high polarity and high aromaticity were recorded in the toluene-insoluble fraction. These findings were also confirmed by estimating the aromaticity degree using the peak under the aliphatic and C=C aromatic areas in the FTIR spectra. It was found that the Algerian Hassi-Messaoud asphaltenes contain low amount of sulfur compared with other types of asphaltenes. Thermogravimetric analysis indicated that the maximum mass loss was recorded at 492, 538, and 557 °C for toluene-insoluble, neat, and toluene-soluble asphaltenes, respectively. Preliminary data from ssNMR has revealed that (AS)_{OR} had different peak shapes compared to (AS)_S and (AS)_{NS} samples. Additionally, the aromatic/aliphatic ratio in (AS)_{OR} sample was lower when compared to the (AS)_S and (AS)_{NS} samples. More interestingly, the (AS)_{NS} sample contained the largest oxygen content which might be in alignment with the


fact that high levels of oxygen contribute to the asphaltene instability. This oxygen content is presented as ketone, aldehyde, or C–O functionality. It could be concluded that the Algerian Hassi-Messaoud asphaltenes have a very complex chemical structure that affects the behavior and stability of the asphaltenes during oil production. According to our findings, the oxygen content could be the driving force for this asphaltene instability.

Acknowledgements

The authors would like to acknowledge funding from le Ministère de l'enseignement supérieur et de la recherche scientifique, and the Chemical and Petroleum Engineering Department at the University of Calgary, Alberta, Canada. A special thanks to Dr. Khodja Mohamed from le centre de recherche et de développement Sonatrach for helping in asphaltenes extraction. Special appreciation to Dr. Patrick van der Wel and the ENTEG Institute, the University of Groningen, for providing access to the ssNMR facility.

ORCID

Abdallah D. Manasrah  <http://orcid.org/0000-0002-2534-1739>

Khaled O. Sebakhy  <http://orcid.org/0000-0001-6620-0951>

Nashaat N. Nassar  <http://orcid.org/0000-0001-9014-542X>

References

- Abbas, H., A. Manasrah, A. A. Saad, K. O. Sebakhy, and Y. Bouhadda. 2021. Adsorption of Algerian asphaltenes onto synthesized maghemite iron oxide nanoparticles. *Petroleum Chemistry* 61 (1):67–75. doi: [10.1134/S0965544121010072](https://doi.org/10.1134/S0965544121010072).
- Acevedo, S., A. Castro, J. G. Negrin, A. Fernández, G. Escobar, V. Piscitelli, F. Delolme, and G. Dessalces. 2007. Relations between asphaltene structures and their physical and chemical properties: The rosary-type structure. *Energy & Fuels* 21 (4):2165–75. doi: [10.1021/ef070089v](https://doi.org/10.1021/ef070089v).
- Acevedo, S., O. Escobar, L. Echevarria, L. B. Gutiérrez, and B. Méndez. 2004. Structural analysis of soluble and insoluble fractions of asphaltenes isolated using the PNP method. Relation between asphaltene structure and solubility. *Energy & Fuels* 18 (2):305–11. doi: [10.1021/ef030065y](https://doi.org/10.1021/ef030065y).
- Adams, J. J. 2014. Asphaltene adsorption, a literature review. *Energy & Fuels* 28 (5): 2831–56. doi: [10.1021/ef500282p](https://doi.org/10.1021/ef500282p).
- Al-Maamari, R. S., and J. S. Buckley. 2003. Asphaltene precipitation and alteration of wetting: The potential for wettability changes during oil production. *SPE Reservoir Evaluation & Engineering* 6 (04):210–4. doi: [10.2118/84938-PA](https://doi.org/10.2118/84938-PA).
- Alian, S. S., A. A. Omar, A. F. Alta'ee, and I. Hani. 2011. *Study of Asphaltene Precipitation induced formation Damage during CO₂ Injection for a Malaysian light oil*. World Academy of Science, Engineering and Technology. 4.0 (6).doi.org/10.5281/zenodo.1331039
- Andersen, S. I., J. O. Jensen, and J. G. Speight. 2005. X-ray diffraction of subfractions of petroleum asphaltenes. *Energy & Fuels* 19 (6):2371–7. doi: [10.1021/ef050039v](https://doi.org/10.1021/ef050039v).
- Bava, Y. B., M. Geronés, D. Buceta, D. de la Iglesia Rodríguez, M. A. López-Quintela, and M. F. Erben. 2019. Elucidation of the average molecular structure of argentinian asphaltenes. *Energy & Fuels* 33 (4):2950–60. doi: [10.1021/acs.energyfuels.8b04318](https://doi.org/10.1021/acs.energyfuels.8b04318).

- Bouhadda, Y., D. Bendedouch, E. Sheu, and A. Krallafa. 2000. Some preliminary results on a physico-chemical characterization of a Hassi Messaoud petroleum asphaltene. *Energy & Fuels* 14 (4):845–53. doi: [10.1021/ef9902092](https://doi.org/10.1021/ef9902092).
- Bouhadda, Y., D. Bormann, E. Sheu, D. Bendedouch, A. Krallafa, and M. Daaou. 2007. Characterization of Algerian Hassi-Messaoud asphaltene structure using Raman spectrometry and X-ray diffraction. *Fuel* 86 (12-13):1855–64. doi: [10.1016/j.fuel.2006.12.006](https://doi.org/10.1016/j.fuel.2006.12.006).
- Bouhadda, Y., P. Florian, D. Bendedouch, T. Fergoug, and D. Bormann. 2010. Determination of Algerian Hassi-Messaoud asphaltene aromaticity with different solid-state NMR sequences. *Fuel* 89 (2):522–6. doi: [10.1016/j.fuel.2009.09.018](https://doi.org/10.1016/j.fuel.2009.09.018).
- Boukherissa, M. 2008. *Etude de la stabilité des asphaltènes dans le pétrole brut: choix de dispersants et le mécanisme d'action*. Université Paul Verlaine-Metz. <https://hal.univ-lorraine.fr/tel-01752594/document>
- Calemma, V., P. Iwanski, M. Nali, R. Scotti, and L. Montanari. 1995. Structural characterization of asphaltenes of different origins. *Energy & Fuels* 9 (2):225–30. doi: [10.1021/ef00050a004](https://doi.org/10.1021/ef00050a004).
- Carbognani, L., J. Espidel, and A. Izquierdo. 2000. *Characterization of asphaltenic deposits from oil production and transportation operations, Developments in petroleum science*. Elsevier, 335–62. [https://doi.org/10.1016/S0376-7361\(09\)70284-5](https://doi.org/10.1016/S0376-7361(09)70284-5)
- Creek, J. L. 2005. Freedom of action in the state of asphaltenes: Escape from conventional wisdom. *Energy & Fuels* 19 (4):1212–24. doi: [10.1021/ef049778m](https://doi.org/10.1021/ef049778m).
- D2892-16, A. 2016. *Standard test method for distillation of crude petroleum (15-Theoretical Plate Column)*, ASTM International. West Conshohocken, PA: ASTM International.
- D5236-13, A. 2013. *Standard test method for distillation of heavy hydrocarbon mixtures (vacuum potstill method)*. *Annual Book of ASTM Standards*. West Conshohocken, PA: ASTM International.
- Daaou, M., D. Bendedouch, Y. Bouhadda, L. Vernex-Loiset, A. Modarressi, and M. Rogalski. 2009. Explaining the flocculation of Hassi Messaoud asphaltenes in terms of structural characteristics of monomers and aggregates. *Energy & Fuels* 23 (11):5556–63. doi: [10.1021/ef900596y](https://doi.org/10.1021/ef900596y).
- Daaou, M., D. Bendedouch, A. Modarressi, and M. Rogalski. 2012. Properties of the polar fraction of Hassi-Messaoud asphaltenes. *Energy & Fuels* 26 (9):5672–8. doi: [10.1021/ef300573d](https://doi.org/10.1021/ef300573d).
- Daaou, M., A. Larbi, B. Martínez-Haya, and M. Rogalski. 2016. A Comparative study of the chemical structure of asphaltenes from Algerian petroleum collected at different stages of extraction and processing. *Journal of Petroleum Science and Engineering* 138:50–6. doi: [10.1016/j.petrol.2015.11.040](https://doi.org/10.1016/j.petrol.2015.11.040).
- Daaou, M., A. Modarressi, D. Bendedouch, Y. Bouhadda, G. Krier, and M. Rogalski. 2008. Characterization of the nonstable fraction of Hassi –Messaoud Asphaltenes. *Energy & Fuels* 22 (5):3134–42. doi: [10.1021/ef800078u](https://doi.org/10.1021/ef800078u).
- DE, G.D.E.D.C. and DE Master, L. E. 2009. République Algérienne Démocratique et Populaire.
- Durand, E., M. Clemancey, J.-M. Lancelin, J. Verstraete, D. Espinat, and A.-A. Quoineaud. 2010. Effect of chemical composition on asphaltenes aggregation. *Energy & Fuels* 24 (2): 1051–62. doi: [10.1021/ef900599v](https://doi.org/10.1021/ef900599v).
- Fergoug, T., and Y. Bouhadda. 2014. Determination of Hassi Messaoud asphaltene aromatic structure from ¹H & ¹³C NMR analysis. *Fuel* 115:521–6. doi: [10.1016/j.fuel.2013.07.055](https://doi.org/10.1016/j.fuel.2013.07.055).
- Fini, E. H., S. Hosseinnézhad, D. J. Oldham, E. Chailleux, and V. Gaudefroy. 2017. Source dependency of rheological and surface characteristics of bio-modified asphalts. *Road Materials and Pavement Design* 18 (2):408–24. doi: [10.1080/14680629.2016.1163281](https://doi.org/10.1080/14680629.2016.1163281).
- Freeman, D., D. C. Saint Martin, and C. Boreham. 1993. Identification of metalloporphyrins by third-derivative UV/VIS diode array spectroscopy. *Energy & Fuels* 7 (2):194–9. doi: [10.1021/ef00038a006](https://doi.org/10.1021/ef00038a006).

- Gowdy, J., and R. Julia. 2007. Technology and petroleum exhaustion: Evidence from two mega-oilfields. *Energy* 32 (8):1448–54. doi: [10.1016/j.energy.2006.10.019](https://doi.org/10.1016/j.energy.2006.10.019).
- Groenzin, H., and O. C. Mullins. 1999. Asphaltene molecular size and structure. *The Journal of Physical Chemistry A* 103 (50):11237–45. doi: [10.1021/jp992609w](https://doi.org/10.1021/jp992609w).
- Groenzin, H., and O. C. Mullins. 2000. Molecular size and structure of asphaltenes from various sources. *Energy & Fuels* 14 (3):677–84. doi: [10.1021/ef990225z](https://doi.org/10.1021/ef990225z).
- Guan, Q., J. C. Chai, A. Goharzadeh, F. M. Vargas, S. L. Biswal, W. G. Chapman, M. Zhang, and Y. F. Yap. 2018. A unidirectional one-dimensional approach for asphaltene deposition in large length-to-diameter ratios scenarios. *Journal of Petroleum Science and Engineering* 166:857–70. doi: [10.1016/j.petrol.2018.03.056](https://doi.org/10.1016/j.petrol.2018.03.056).
- Gutiérrez, L. B., M. A. Ranaudo, B. Méndez, and S. Acevedo. 2001. Fractionation of asphaltene by complex formation with p-nitrophenol. A method for structural studies and stability of asphaltene colloids. *Energy & Fuels* 15 (3):624–8. doi: [10.1021/ef000180y](https://doi.org/10.1021/ef000180y).
- Haskett, C. E., and M. Tartera. 1965. A practical solution to the problem of asphaltene deposits-Hassi Messaoud Field, Algeria. *Journal of Petroleum Technology* 17 (04):387–91. doi: [10.2118/994-PA](https://doi.org/10.2118/994-PA).
- Hung, A. M., M. Mousavi, F. Pahlavan, and E. H. Fini. 2017. Intermolecular interactions of isolated bio-oil compounds and their effect on bitumen interfaces. *ACS Sustainable Chemistry & Engineering* 5 (9):7920–31. doi: [10.1021/acssuschemeng.7b01462](https://doi.org/10.1021/acssuschemeng.7b01462).
- Kam'yanov, V. F., Bodraya, N. V., Sivirilov, P. P., Unger, F. G., Filimonova, T. A., & Chernyavskii, V. N. 1989. X-ray diffraction analysis of the resinous-asphaltene components of West Siberian crude oil. *Petroleum Chemistry USSR* 29 (1):1–13.
- Larbi, A., M. Daaou, and A. Faraoun. 2015. Investigation of structural parameters and self-aggregation of Algerian asphaltenes in organic solvents. *Petroleum Science* 12 (3):509–17. doi: [10.1007/s12182-015-0041-x](https://doi.org/10.1007/s12182-015-0041-x).
- Lei, Y., H. Wang, X. Chen, X. Yang, Z. You, S. Dong, and J. Gao. 2018. Shear property, high-temperature rheological performance and low-temperature flexibility of asphalt mastics modified with bio-oil. *Construction and Building Materials* 174:30–7. doi: [10.1016/j.conbuildmat.2018.04.094](https://doi.org/10.1016/j.conbuildmat.2018.04.094).
- Leontaritis, K., J. Amaefule, and R. Charles. 1994. A systematic approach for the prevention and treatment of formation damage caused by asphaltene deposition. *SPE Production & Facilities* 9 (03):157–64. doi: [10.2118/23810-PA](https://doi.org/10.2118/23810-PA).
- Leyva, C., J. Ancheyta, C. Berruenco, and M. Millán. 2013. Chemical characterization of asphaltenes from various crude oils. *Fuel Processing Technology* 106:734–8. doi: [10.1016/j.fuproc.2012.10.009](https://doi.org/10.1016/j.fuproc.2012.10.009).
- Lindon, J. C., G. E. Tranter, and D. Koppenaal. 2016. *Encyclopedia of spectroscopy and spectrometry*. Academic Press. <https://www.elsevier.com/books/encyclopedia-of-spectroscopy-and-spectrometry/lindon/978-0-12-803224-4>
- Manasrah, A. D., A. Hassan, and N. N. Nassar. 2019a. Enhancement of petroleum coke thermal reactivity using Oxy-cracking technique. *The Canadian Journal of Chemical Engineering* 97 (11):2794–803. doi: [10.1002/cjce.23574](https://doi.org/10.1002/cjce.23574).
- Manasrah, A. D., and N. N. Nassar. 2020. Oxy-cracking technique for producing non-combustion products from residual feedstocks and cleaning up wastewater. *Applied Energy* 280:115890. doi: [10.1016/j.apenergy.2020.115890](https://doi.org/10.1016/j.apenergy.2020.115890).
- Manasrah, A. D., N. N. Nassar, and L. C. Ortega. 2018. Conversion of petroleum coke into valuable products using oxy-cracking technique. *Fuel* 215:865–78. doi: [10.1016/j.fuel.2017.11.103](https://doi.org/10.1016/j.fuel.2017.11.103).
- Manasrah, A. D., G. Vitale, and N. N. Nassar. 2019b. Catalytic oxy-cracking of petroleum coke on copper silicate for production of humic acids. *Applied Catalysis B: Environmental* 264:118472. doi: [10.1016/j.apcatb.2019.118472](https://doi.org/10.1016/j.apcatb.2019.118472).

- Maqbool, T., A. T. Balgoa, and H. S. Fogler. 2009. Revisiting asphaltene precipitation from crude oils: A case of neglected kinetic effects. *Energy & Fuels* 23 (7):3681–6. doi: [10.1021/ef9002236](https://doi.org/10.1021/ef9002236).
- Medina, O. E., J. Gallego, N. N. Nassar, S. A. Acevedo, F. B. Cortés, and C. A. Franco. 2020. Thermo-oxidative decomposition behaviors of different sources of n-C7 Asphaltenes under high-pressure conditions. *Energy & Fuels* 34 (7):8740–58. doi: [10.1021/acs.energyfuels.0c01234](https://doi.org/10.1021/acs.energyfuels.0c01234).
- Middtum, Ø. 1999. A physical-Chemical and chemometric study of interfacially active components in crude oils. PhD. diss., University of Bergen, Norway.
- Mohammadi, M., M. Dadvar, and B. Dabir. 2017. TiO₂/SiO₂ nanofluids as novel inhibitors for the stability of asphaltene particles in crude oil: Mechanistic understanding, screening, modeling, and optimization. *Journal of Molecular Liquids* 238:326–40. doi: [10.1016/j.molliq.2017.05.014](https://doi.org/10.1016/j.molliq.2017.05.014).
- Mullins, O. C. 2011. The asphaltenes. *Annual Review of Analytical Chemistry. Annual Reviews* 4: 393–418. doi: [10.1146/annurev-anchem-061010-113849](https://doi.org/10.1146/annurev-anchem-061010-113849)
- Mullins, O. C., H. Sabbah, J. Eyssautier, A. E. Pomerantz, L. Barré, A. B. Andrews, Y. Ruiz-Morales, F. Mostowfi, R. McFarlane, L. Goual, et al. 2012. Advances in asphaltene science and the Yen–Mullins model. *Energy & Fuels* 26 (7):3986–4003. doi: [10.1021/ef300185p](https://doi.org/10.1021/ef300185p).
- Murgich, J. 2003. Molecular simulation and the aggregation of the heavy fractions in crude oils. *Molecular Simulation* 29 (6-7):451–61. doi: [10.1080/0892702031000148762](https://doi.org/10.1080/0892702031000148762).
- Mustafin, R., A. D. Manasrah, G. Vitale, R. Askari, and N. N. Nassar. 2020. Enhanced thermal conductivity and reduced viscosity of aegirine-based VR/VGO nanofluids for enhanced thermal oil recovery application. *Journal of Petroleum Science and Engineering* 185:106569. doi: [10.1016/j.petrol.2019.106569](https://doi.org/10.1016/j.petrol.2019.106569).
- Nassar, N. N., A. Hassan, and P. Pereira-Almao. 2011. Application of nanotechnology for heavy oil upgrading: Catalytic steam gasification/cracking of asphaltenes. *Energy & Fuels* 25 (4):1566–70. [Database] doi: [10.1021/ef2001772](https://doi.org/10.1021/ef2001772).
- Sagar, A. D. 2005. Alleviating energy poverty for the world's poor. *Energy Policy* 33 (11): 1367–72. doi: [10.1016/j.enpol.2004.01.001](https://doi.org/10.1016/j.enpol.2004.01.001).
- Schuler, B., S. Fatayer, G. Meyer, E. Rogel, M. Moir, Y. Zhang, M. R. Harper, A. E. Pomerantz, K. D. Bake, M. Witt, et al. 2017a. Heavy oil based mixtures of different origins and treatments studied by atomic force microscopy. *Energy & Fuels* 31 (7):6856–61. doi: [10.1021/acs.energyfuels.7b00805](https://doi.org/10.1021/acs.energyfuels.7b00805).
- Schuler, B., G. Meyer, D. Peña, O. C. Mullins, and L. Gross. 2015. Unraveling the molecular structures of asphaltenes by atomic force microscopy. *Journal of the American Chemical Society* 137 (31):9870–6. doi: [10.1021/jacs.5b04056](https://doi.org/10.1021/jacs.5b04056).
- Schuler, B., Y. Zhang, S. Collazos, S. Fatayer, G. Meyer, D. Pérez, E. Guitián, M. R. Harper, J. D. Kushnerick, D. Peña, et al. 2017b. Characterizing aliphatic moieties in hydrocarbons with atomic force microscopy. *Chemical Science* 8 (3):2315–20. doi: [10.1039/c6sc04698c](https://doi.org/10.1039/c6sc04698c).
- Schuler, B., Y. Zhang, F. Liu, A. E. Pomerantz, A. B. Andrews, L. Gross, V. Pauchard, S. Banerjee, and O. C. Mullins. 2020. Overview of asphaltene nanostructures and thermodynamic applications. *Energy & Fuels* 34 (12):15082–105. doi: [10.1021/acs.energyfuels.0c00874](https://doi.org/10.1021/acs.energyfuels.0c00874).
- Shirokoff, J. W., M. N. Siddiqui, and M. F. Ali. 1997. Characterization of the structure of Saudi crude asphaltenes by X-ray diffraction. *Energy & Fuels* 11 (3):561–5. doi: [10.1021/ef960025c](https://doi.org/10.1021/ef960025c).
- Siddiqui, M. N., M. F. Ali, and J. Shirokoff. 2002. Use of X-ray diffraction in assessing the aging pattern of asphalt fractions. *Fuel* 81 (1):51–8. doi: [10.1016/S0016-2361\(01\)00116-8](https://doi.org/10.1016/S0016-2361(01)00116-8).
- Spiecker, P. M., K. L. Gawrys, and P. K. Kilpatrick. 2003. Aggregation and solubility behavior of asphaltenes and their subfractions. *Journal of Colloid and Interface Science* 267 (1): 178–93. doi: [10.1016/S0021-9797\(03\)00641-6](https://doi.org/10.1016/S0021-9797(03)00641-6).

- Strausz, O. P., T. W. Mojelsky, and E. M. Lown. 1992. The molecular structure of asphaltene: An unfolding story. *Fuel* 71 (12):1355–63. doi: [10.1016/0016-2361\(92\)90206-4](https://doi.org/10.1016/0016-2361(92)90206-4).
- Trejo, F., M. S. Rana, and J. Ancheyta. 2010. Thermogravimetric determination of coke from asphaltenes, resins and sediments and coking kinetics of heavy crude asphaltenes. *Catalysis Today* 150 (3-4):272–8. doi: [10.1016/j.cattod.2009.07.091](https://doi.org/10.1016/j.cattod.2009.07.091).
- Trimm, D. 1996. *Catalytic deactivation, studies in surface science and catalysis*, 65–76. Elsevier. [https://doi.org/10.1016/S0167-2991\(96\)80008-5](https://doi.org/10.1016/S0167-2991(96)80008-5)
- Yao, B., W. Chen, C. Li, F. Yang, G. Sun, G. Wang, and H. Xu. 2020. Polar asphaltenes facilitate the flow improving performance of polyethylene-vinyl acetate. *Fuel Processing Technology* 207:106481. doi: [10.1016/j.fuproc.2020.106481](https://doi.org/10.1016/j.fuproc.2020.106481).
- Yen, T. F., J. G. Erdman, and S. S. Pollack. 1961. Investigation of the structure of petroleum asphaltenes by X-ray diffraction. *Analytical Chemistry* 33 (11):1587–94. doi: [10.1021/ac60179a039](https://doi.org/10.1021/ac60179a039).
- Yoon, S. S. D., Bhatt, W. Lee, H. Y. Lee, S. Y. Jeong, J.-O. Baeg, and C. W. Lee. 2009. Separation and characterization of bitumen from Athabasca oil sand. *Korean Journal of Chemical Engineering* 26 (1):64–71. doi: [10.1007/s11814-009-0011-3](https://doi.org/10.1007/s11814-009-0011-3).

Nomenclature

(AS) _{OR}	the neat asphaltenes
(AS) _S	soluble fraction in toluene
(AS) _{NS}	insoluble fraction
A ₃ /A ₁	the corresponding aromatic index
A ₂ /A ₁	the carbonyl index
f _a	the aromaticity
A	the integrated area under the corresponding peak
λ	1.54059 Å
θ ₀₀₂ , θ _γ , and θ ₁₀	the diffraction angles at 002, γ and 10 bands, respectively
ω	the full width at half maximum (FWHM)
d _m	the distance between two aromatic sheets
d _γ	the distance between the two aliphatic chains or saturated rings
L _a	the diameter of the aromatic sheet
L _c	the average height of the crystallite
M	the average number of aromatic sheets
R _a	the average number of aromatic rings in each aromatic sheet
C _{AU}	the number of carbons per aromatic structural
PANU	the polycyclic aromatic and naphthenic units